Method for the determination of preferential orientation of marine particles from laser diffraction measurements

J. S. Font-Munoz, Raphael Jeanneret, Idan Tuval, Gotzon Basterretxea

Research Article | Vol. 28, No. 9 / 27 April 2020 / Optics Express 14085
Optics EXPRESS

Method for the determination of preferential orientation of marine particles from laser diffraction measurements

JOAN S. FONT-MUÑOZ,[1,2,*] RAPHAËL JEANNERET,[3] IDAN TUVAL,[4,5] AND GOTZON BASTERRETXEA[4]

[1]IFREMER, French Institute for Sea Research, DYNECO PELAGOS, 29280, Plouzané, France
[2]Université de Brest - UBO/CNRS/IFREMER/IRD, 29238, Brest, France
[3]Laboratoire de Physique de l'Ecole normale supérieure, ENS, Université PSL, CNRS, Sorbonne Université, Université de Paris, F-75005 Paris, France
[4]Dept. of Marine Ecology. IMEDEA (UIB-CSIC). Miquel Marques 21, 07190. Esporles, Balearic Islands, Spain
[5]Dept. of Physics. University of the Balearic Islands, Ctra. Valldemossa Km. 7.5, 07122, Palma, Balearic Islands, Spain
[*]jsfontmu@ifremer.fr

Abstract: In situ laser diffractometry (LD) is increasingly used in oceanographic studies to estimate sediment transport, particle fluxes and to assess the concentration of marine phytoplankton. It enables an accurate characterization of the size distribution of suspended particles from the scattering signal produced by their interaction with a collimated laser beam. LD reliably reflects the sizes of suspensions dominated by nearly spherical particles; however, when complex particle morphologies dominate the suspension (e.g. phytoplankton) the resulting particle size distribution (PSD) may present significant variations attributed to different factors. In particular, the orientation of non-spherical particles - which abound in the sea – modifies LD measurements of PSDs. While this may be interpreted as a drawback for some studies (i.e. when precise measurement of the volume concentration is required), we propose that detailed analysis of this signal provides information on particle orientation. We use PDMS micropillars with prescribed elliptical cross-sections to experimentally determine the dependence between the spatial orientation of elongated particles and changes in the PSD measured with a LISST laser diffractometer. We show that LD can be used to adequately characterize the different dimensions of the non-spherical particles at specific orientations. Using this property, we describe and validate a method to infer the preferential orientation of particles in the sea. Our study opens new perspectives in the use of in-situ LD in ocean research.

1. Introduction

The characterization of biotic and abiotic particle size distributions (PSD) in natural waters is essential for a wide variety of scientific disciplines, ranging from ocean optics [1] and biological oceanography [2,3] to sediment dynamics and marine geochemistry [4,5]. Absorption and scattering by suspended particles strongly affect light propagation in the sea, thereby regulating the availability of light for photosynthesis [6] and influencing ocean color information acquired by remote sensing [7]. Suspended particles also influence trophic interactions within the planktonic community, provide a habitat for microbial communities [8,9] and modulate vertical fluxes of major biogeochemical components, pollutants, and contaminants [10–12]. These effects have enormous interest for the understanding, prediction and management of the marine environment.

The distribution, size and shape of marine particles, including phytoplankton, are routinely addressed by different methods including microscopy, electrical resistance sensing, optical diffractometry and flow cytometry [13–16]. Some instruments allow determination of particles

#390388 https://doi.org/10.1364/OE.390388
Journal © 2020 Received 12 Feb 2020; revised 8 Apr 2020; accepted 8 Apr 2020; published 24 Apr 2020

Optics EXPRESS

without further sample manipulation and hence providing detailed information (i.e. concentration and size structure) of suspended sediments and plankton in the natural environment. Among these, laser diffractometers are unique in that they are able to characterize the particles in suspension from the angular distribution of a forward scattered coherent light and their use as a suitable technique is rapidly expanding [17,18]. Several commercial in-situ operating instruments such as the Multi-Angle Scattering Optical Tool (MASCOT) or the Laser In-Situ Scattering and Transmissiometry (LISST) are based on this principle [19,20]. These instruments are now routinely used for sediment and plankton studies [21–23].

Laser diffraction measurements require the use of an optical model - based on either analytical theory or empirical data - in order to predict the distribution of light scattered by particles of a specific size in the range of angles measured by the photodetectors of the instrument and, in that sense, it is an indirect method [19,24]. The majority of LD instruments use Mie theory for conversion from scattering to particle concentration and size. This theory provides exact solutions to Maxwell's equations for the problem of light propagation and diffraction from a spherical obstacle without a priori imposed restrictions on particle size [25] . According to Mie theory, the light intensity pattern resulting from the interaction depends on the wavelength of the incident light, the dispersion angle considered, the particle diameter and its refractive index [26]. A drawback for its use in marine samples is that many planktonic organisms and particle aggregates present in seawater are of elongated forms, hence biasing LD measurements when they represent a dominant fraction of suspended matter. When Mie theory is applied to characterize these suspensions (e.g. a population of pennate diatoms), the PSD displays peaks that appear to be related to the different axes of symmetry of the particles [2,27]. We will demonstrate that in these cases LD provides information on particle orientation if size characteristics are known.

Theoretical studies of the light-scattering properties of non-spherical particles show that their optical properties particularly deviate from those of spheres of the same volume as the optical size increases) [28,29]. This is especially relevant in the case of large phytoplankton cells (i.e. microphytoplankton) that often exhibit complex shapes or elongated morphologies with length:width aspect ratios >5 [30]. In these cases, the intensity distribution of the scattered light depends strongly on the orientation of the particles with respect to the incident beam [1,28,31] and, ultimately, on the cross section of the particles in the plane perpendicular to the beam [32–34].

In the sea, hydrodynamic shear can induce phytoplankton cell alignment with respect to local flows [35]. Likewise, in sufficiently quiescent environments, the force of gravity can vertically orient cell chains and particle aggregates [13]. Although evidences of these phenomena in the natural environment are still scarce, recent studies show that preferential orientation of marine particles may be more prevalent than previously believed [36–39]. Here, we describe a procedure for inferring preferential particle orientation in the sea from the PSD spectrum obtained using in-situ LD. This method requires knowledge of the approximate dimensions of the particles and, thus, is best suited for the determination of phytoplankton orientation for which these can be easily assessed by concurrent microscopy measurements. We use the diffraction signal provided by a LISST-100X (Sequoia Scientific Inc.) laser diffractometer in a series of experiments carried out using artificially constructed micropatterns to analyze the dependence of PSD spectrum variations on the orientation of non-spherical particles, therefore providing a direct methodology for assessing the orientation of particles in the sea.

2. Material and methods

Laser diffractometry allows estimating the PSD of the particles suspended in water. When crossing the sample volume, the laser beam gets deviated by the particles, creating a scattering pattern, which, in the particular case of the forward diffraction problem, is related to the size of the particles. Usually, a detector array captures this diffraction and then used to solve a matrix

Optics EXPRESS

equation that provides a volume concentration as function of equivalent spherical diameter (ESD), for which it is normally assumed that the particles in suspension are spheres [19]. In particular LISST obtains the particle volume concentration by size ranges (i.e. volume of particles in the seawater per unit volume of seawater) using Mie theory. This instrument uses a 670 nm collimated laser beam to illuminate the suspended particles and a partial-arc detector measures the intensity of the scattered light, corresponding to 32 different size classes logarithmically spaced from 2.5 to 500 µm [19,24]. In this size range, the light scattering pattern in small angles is determined mainly by the size of the particles and by their refractive index [40].

As illustrated in Fig. 1, (a) spheroidal particle oriented at a certain angle ψ with respect to the light direction is expected to scatter light in the same way as a particle having the dimensions of its projection onto the plane perpendicular to the beam [32–34]. We use this property to study in detail the influence of particle orientation on the PSD measured by laser diffractometry. To keep the particles oriented at a certain angle ψ with respect to the incident beam, we use polydimethylsiloxane (PDMS) micropillars randomly distributed on a PDMS plate (see Fig. 1(c) and Appendix Fig. 7). Each PDMS plate was inserted vertically (θ=0) into the LISST-100X sample chamber filled with pure (Milli-q) water where steady LD measurements were taken over 60s intervals.

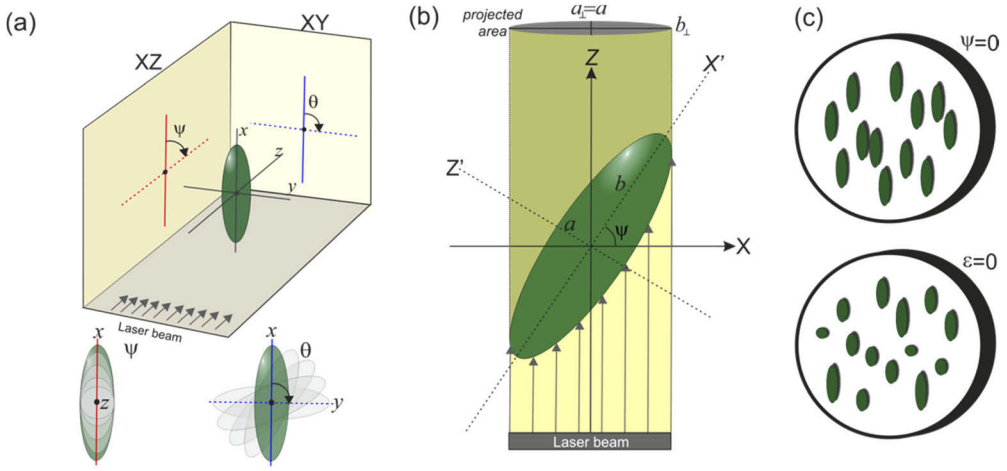

Fig. 1. (a) 3D perspective view of a prolate spheroidal particle and its corresponding projections (below) in the XZ (ψ angle rotation) and XY planes (θ angle rotation). (b) XZ plane view: the major spheroidal axis b forms an angle ψ with the x-axis in the orthogonal XY plane while oriented with an angle θ with respect to that same plane, where the projected ellipse has $b_\perp$ and $a_\perp = a$ as major and minor axis, respectively. (c) PDMS chips with a uniform (top) and non-uniform (bottom) orientational distribution ($\psi = 0$ and ε=0, respectively).

PDMS is an elastomer with excellent optical properties that is commonly used in microfluidic applications. In addition, its refractive index (normalized by that of sea water) is ~1.06 which falls within the typical range of phytoplankton cells (1.02-1.07) [40]. The thin PDMS plates engraved on one side with arrays of cylindrical pillars (with elliptical cross-section) were made using standard soft photo-lithography techniques. The primary molds used to obtain the PDMS plates were made using conventional glass slides onto which the opposite pattern was printed with SU-8 photoresist (GM 1060; Gersteltec Sàrl) giving a final thickness ~15 µm (which is also the final thickness of the pillars appearing on the PDMS). The patterns on the transparency masks used to print the primary molds were generated using Matlab software.

Optics EXPRESS

In order to develop a methodology for analyzing the influence of particle orientation in the LD signal, we carried out experiments with two sets of PDMS plates: a first set consisting of 7 plates of pillars having constant elliptical cross-section with a minor axis a=15 μm and a major axis length ($b_\perp$) varying from 15 to 75 μm in steps of 10 μm and constant in-plane orientation (Table 1). These patterns were used to experimentally mimic 7 different projections in the XY plane (Fig. 1(b) and Appendix, Fig. 7 left) of identical spheroidal particles having all exactly the same predefined orientation (ψ, Fig. 1(c)). A second set of 5 PDMS plates was built to study the case of non-uniform ψ orientation distributions and consisted of pillars with continuously modulated elliptical cross-section with $b_\perp$ varying from 15 to 75 μm, a=15 μm and constant in-plane orientation (Fig. 1(d)). These plates are described by a single parameter ε that accounts for the degree of randomness in ψ, where ε=0 indicates uniform random orientations, ε=-1 pillars mostly oriented with the major axis parallel to the beam, and ε=+1 pillars mostly oriented with the major axis perpendicular to the beam. These patterns were used to experimentally mimic identical spheroidal particles oriented with a distribution of ψ following $P(\psi) = [1 + \varepsilon \cos(2\psi)]/\pi$, which results in the length $b_\perp$ of the projected in-plane ellipses to be taken from the distribution

$$P(b_\perp) = \frac{1}{b-a}\left[1 - \varepsilon \cos\left(\pi \frac{b_\perp - a}{b-a}\right)\right].$$

We varied the parameter ε from ε=-1 to 1 in steps of 0.5, resulting in a total of 5 different patterns. In all cases, the pillars were randomly positioned within the PDMS plates in order to only extract information on the elliptical pillars (and not on an underlying structure of the array of pillars) from the LD experiments. Finally, we made the arrays such that the pillars never overlapped and with an average distance between the (edge of the) pillars d=150 μm (giving surface coverages of the pillars between ~2 and 6% depending on the specific pattern).

Table 1. Size of the major axis and minor axis of the micropillars for each of the 7 orientations in the XZ plane.

ψ	90°	70.5°	62.18°	53.1°	42.8°	29.9°	0°
$b_\perp$	15μm	25μm	35μm	45μm	55μm	65μm	75μm
a	15μm	15μm	15μm	15μm	15μm	15μm	15μm

3. Results and assessment

3.1. Variations in PSD define off-plane particle orientations

The normalized PSD for uniformly oriented elongated particles is shown in Fig. 2(a). For all 7 PDMS plates tested, it is characterized by a well-defined peak for size channels associated with the diffraction pattern of the respective projection of the spheroid major axis. In fact, the position of the main peak clearly sweeps the different size-channels within the range [a, b] for the different values of ψ (or the equivalent values of the in-plane projected major axis $b_\perp$; see Table 1) and, although showing a slight tendency for underestimating $b_\perp$, it is very well captured by a linear nearly 1:1 fit (r = 0.92) (Fig. 2(c)). This simple and highly accurate relation allows for a direct estimate of exact off-plane orientation from LD measurements if particle size is known, with errors below 5%.

Similarly, for particle distributions with non-uniform off-plane orientations there is a significant correlation (r = 0.90) between the average in-plane projection of particles $< b_\perp >$ and the different values of ε (Fig. 2(d)), although they generically result in wider spectral peaks in the PSD (Fig. 2(b)). Once again, however, $< b_\perp >$ is consistently underestimated with notable deviation from a 1:1 fit for the larger size channels. This is likely due to the non-negligible contributions of projections with smaller $b_\perp$ than $< b_\perp >$ to the overall signal. Nonetheless, these contributions can

Optics EXPRESS

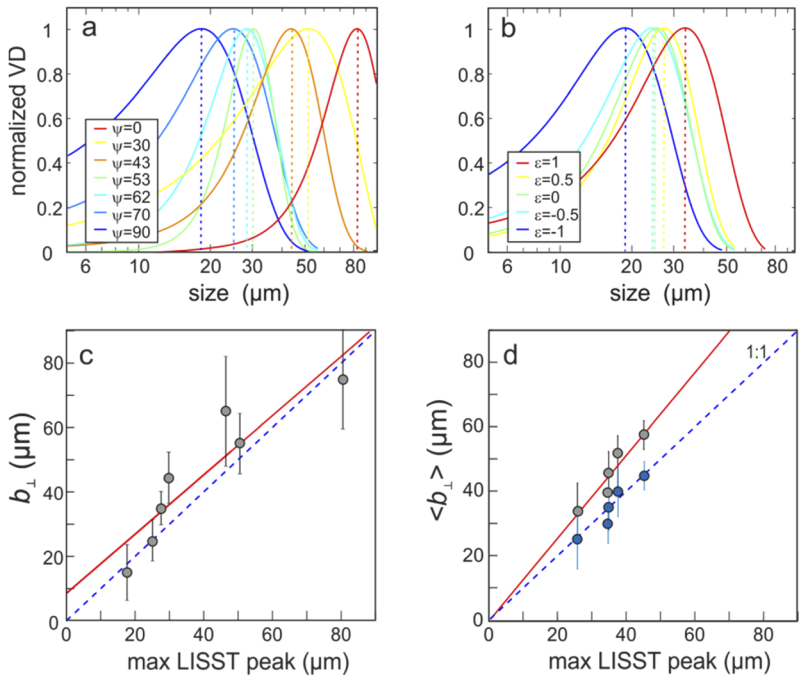

Fig. 2. Normalized PSDs from (a) the 7 PDMS plates with uniform off-plane orientations $\psi \in [0, 90]$ (red to blue), and (b) from the 5 PDMS plates with non-uniform off-plane distributions, i.e. $\varepsilon = [+1{:}0.5{:}{-1}]$ (red to blue). (c) The linear dependence between the position of the main peak of the measured PSDs and $b_\perp$ for uniform ψ; and (d) for non-uniform ψ with $< b_\perp >$. In red the linear fit to the experimental data; in blue the 1:1 reference slope. according to the linear relationship between the major axis and the minor axis, adjusting it only once for the case $\varepsilon = 0$.

be accounted for by using the uniformly random case (ε=0) to fit a single scaling parameter that allows weighting differently the contributions to the signal from major and minor axis. By this simple rescaling we recover a 1:1 relationship with the measured values for all ε (r = 0.98; Fig. 2(d)). Thus, the PSD signal can still be effectively used to estimate average off-plane projection $< b_\perp >$ even in cases with highly non-uniform distributions.

An interesting feature of the PSD for elongated particle shapes is the relationship between the ratio of the diffraction signal (in particle volume concentration, VD) captured at two different size-channels (i.e. $r_{12} = \mathrm{VD}_{ch1}{:}\mathrm{VD}_{ch2}$) and the particle orientation in the XZ plane. For *ch1*=a and *ch2*=$b_\perp$, this relationship is well fitted by a negative exponential (r=-0.92, p<0.01; Fig. 3(a)). A similar relationship (r=-0.90, p<0.01) is obtained if the ratio is calculated between the value obtained by the PSD at the position of the major axis (*ch1*=a) and that returned by the PSD at the position of the major axis of the spheroidal particle (*ch2*=b; Fig. 3(b)).

The described functional relationships allow inferring the orientation of the particles with respect to the incident beam using either the measured position of the spectral peak or equivalently r_{ab}. This ratio was indeed already used as a proxy for orientation in Font-Muñoz et al. (2019) and, as we shall see below, it is a more generally convenient - although less accurate - parametrization of orientational order than the direct measure of the spectral peaks.

Optics EXPRESS

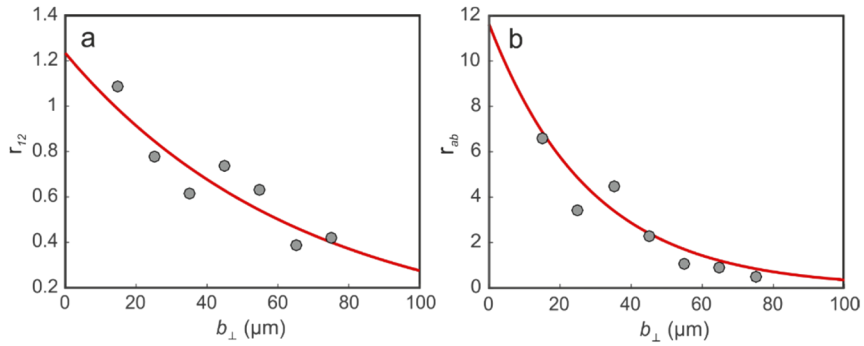

Fig. 3. a) The ratio of the diffraction signal r_{12} for the size of the minor axis (*ch1*=a) and the size of the projected major axis (*ch2*=$b_\perp$) of the micropillars with respect to $b_\perp$ for the different orientations ψ. b) The ratio of the diffraction signal r_{ab} but for *ch1*=a and *ch2*=b as a function of $b_\perp$.

3.2. PSD measurements with LISST depend on in-plane particle orientations

Although, theoretically, the rotation of spheroidal diffracting particles in the XY plane should produce only negligible effects on *LD* signal - since the interference with the laser beam preserves azimuthal symmetry - this is not the case when using LISST. Distinct orientations in θ do in fact produce significant variations in measured VD due to the internal geometric configuration of the LISST optical detectors. These alternate concentric, but only partially overlapping, ring sections of different size ranges (32 rings) break the azimuthal symmetry of the diffracting light [41]. In order to better characterize the measured diffraction signal for the specific arrangement of the LISST photodetectors, we repeated the experiments described in the previous section but for 35 different orientations in the XY plane (i.e. values of θ, Fig. 1(b)).

As shown in Fig. 4, rotation of the micropillars in the *XY* plane yields marked variations for each of the 7 ψ angles analyzed, with peak spectral values varying between a and $b_\perp$ depending on θ (see also Fig. 5(a)). At high ψ orientations (i.e. $\psi = 90°$), when the particles are aligned with the laser beam, a (and thus $b_\perp$=a) is well determined. However, gentle oscillations between a and $b_\perp$ occur at lower ψ (i.e. $\psi = 70.5°$ and 62.2°). Fluctuations in the detected size become more critical with decreasing ψ, with apparent discontinuous transitions from a to $b_\perp$ as we sweep θ for ψ <45°. Mean variations nonetheless show a clear periodic behavior (Fig. 4), with in-plane orientations close to 0° (or 180°) presenting PSD maxima approaching b, while PSD maxima in size-channels close to a occur at orientations ~90° (or ~270°). Results from the 5 PDMS plates with varying degree of non-uniform off-plane orientational distribution of micropillars (i.e. ε) are similarly consistent (see Appendix, Fig. 8 and 9), with θ-dependent spectral peak values bounded between a and $< b_\perp >$ and with the normalized size values revealing a periodic azimuthal variation (Appendix, Fig. 10).

3.3. In-plane average PSD data validates off-plane particle orientations

Our experiments reveal a predominance of the signal of the small axis of the elliptical projections (i.e. a) in the θ-dependent size spectra (see Appendix, Figs. 11 and 12). This is clearly observed in the normalized mean shown in Fig. 4, where maximum values only reach 0.6 instead of the expected value of 1 (=b). This is further evidenced in Fig. 2(c) where, despite the good correlation between the spectral peak and $b_\perp$ ($r = 0.91$, $p<0.01$), the value of $b_\perp$ is slightly underestimated for any ψ. Indeed, when all θ angles are averaged (i.e. assuming cells are randomly oriented in the XY plane) the PSD displays a unimodal distribution with a peak providing information only about the minor axis of the pillars (a=15μm) although with a slight overestimation produced by

Optics EXPRESS

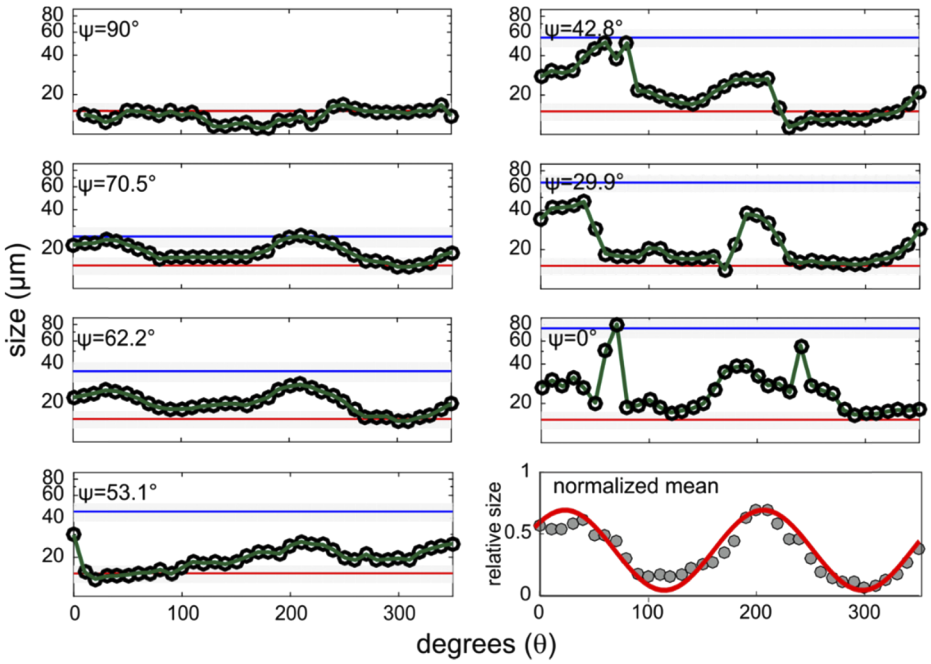

Fig. 4. Position of the main peak of the PSD for each θ orientation of the PDMS plates in the XY plane. Each panel corresponds to a to a different PDMS plate containing pillars with distinct ψ orientation in the XZ plane. The normalized mean size varying from 0(=a) to 1(=b) for each θ orientation is shown in the bottom right panel. The red line corresponds to a sinusoidal fit of the data. The red and blue lines indicate the sizes of the major a and minor axes $b_{\perp}$ of the corresponding projectionsψ.

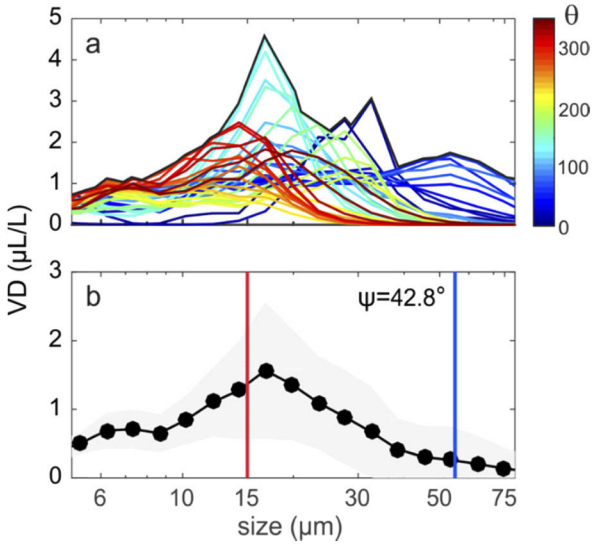

Fig. 5. a) Variation of the size spectrum with θ alignment for ψ=42.8°. The black line represents de envelope. b) Mean spectrum. The red and blue lines represent a and $b_{\perp}$ dimensions. The shaded area marks the mean ± std.

Optics EXPRESS

the displacement of the peak towards larger sizes ($\bar{a}$=16.8 ± 2.8 µm, Fig. 5). Conversely, $b_\perp$ is smeared out in the averaging and, even though its signal could be obtained by different methods (i.e. by gaussian decomposition of the spectrum) its dimension is highly influenced by the weight of a, and thus, underestimated.

If, as it is usually the case for *in situ* observations, we only have access to θ-averaged PSDs, the blurring of the diffraction signal from $b_\perp$ limits substantially the validity of the method discussed above (see Sec. 3.1) for inferring the orientation of the particles with respect to the incident beam based on the measured position of the spectral peak when using LISST. To overcome this drawback, we make use of all our measured θ-averaged spectra to fit an empirical 2D function for the ratio r_{12}= $r_{12}(\psi, ch2)$. The fitted bilinear (planar) function shown in Fig. 6(a), provides a good approximation to the measured values (with r=0.92) but with large residuals for large size-channels (i.e. $ch2 \sim b$). Hence, after inverting conveniently the fitted function, we can use measured r_{12} values at specific size-channels to estimate off-plane orientations ψ=$\psi(r_{12}, ch2)$. Moreover, the use of small *ch2* (i.e. close to a) guarantees an accurate representation of our empirical data (Fig. 6(b)).

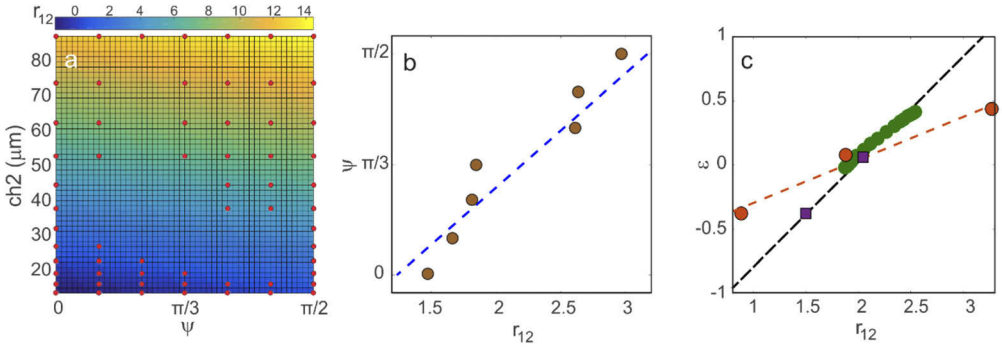

Fig. 6. (a) 2D bilinear fit of $r_{12}(\psi, ch2)$. (b) The inverted linear function ψ (r_{12}, ch2 = 32.54 µm) allows for an accurate estimate of the off-plane orientation ψ based solely on r_{12} values. (c) r_{12} ratios measured with LISST-100X for *Pseudo-nitzschia sp.* (squares from Rienecker et al. 2008; green dots from Font-Muñoz et al. 2019) and *Phaeodactylum tricornutum* (orange dots from Font-Muñoz et al. 2019). Black dashed line is ε (r_{12}, ch2 = 32.54 µm). Orange dashed line is a linear fit to the measured data from *P. tricornutum*.

We further validate this method by comparing previous calculations of non-uniform orientations of elongated cells and published PSD data with the estimates of the technique discussed herein. For instance, our method compares well with previously reported values of preferential orientation in waters dominated by *Pseudo-nitzschia sp*. cells (i.e. during a bloom), whose sizes are compatible with those of our PDMS pillars. Moreover, comparison between lab and field measurements [2] suggests a slight preferential orientation for *in situ* conditions (Fig. 6(c)), a scenario fully compatible with known biophysical mechanisms capable of inducing preferential orientations in the sea. Finally, even for cells in a very different size range but with similar aspect ratio, such as *Phaeodactylum tricornutum* grown in lab cultures, our estimates provide a good qualitative hint of preferential order (i.e. identifying random from mostly horizontal/vertical arrangements) under different levels of artificial agitation.

4. Conclusions

In situ laser diffractometry is a method with high applicability to the study of suspended particles in the marine environment. It provides detailed characterization of particle size and abundance. Here, we expand the sampling capabilities of LD to the estimation of preferential particle

Optics EXPRESS

orientation in the sea that can contribute to the understanding of key processes in the fields of marine optics and plankton ecology. The influence of variations in particle orientation on light propagation in the sea are as important as other well-known factors such as particle rugosity or composition [42]. Indeed, full quantification of the errors associated with scattering from complex particles requires information on particle orientation. Likewise, cell orientation intervenes in key biological processes such as the formation of thin layers or cell pairing [38,39,43].

Our analysis reveals the influence of non-spherical particles in the PSD, which allow us to implement a method to assess preferential particle orientations in the sea from LD measurements. We found that variations in the PSD can be used to obtain valuable information on the preferential orientation of the particles in suspension. In the general case (section 3.1), ψ can be accurately estimated to within 5% (Fig. 2(c)). While the provided methodology is limited to rather homogeneous suspensions, and knowledge on the dimensions of the particles is necessary, it provides highly valuable information for phytoplankton and particle dynamics. Moreover, this is frequently the case of pennate diatom blooms, where it is possible to obtain information on the orientation of the particles by analyzing the size of the particles from discrete samples –i.e. using light microscopy- and measurements of laser diffractometry.

LISST hardware specifically, which was designed for other purposes, presents some limitations for accurate estimation of ψ. This obliges to use an empirical bilinear function (Fig. 6(a)) that reduces the accuracy of ψ estimations to within 10%. Nevertheless, even in this case, the estimated orientations following herein presented methodology should be adequate for most applications, even in cases where cell sizes are markedly distinct from the range used to fit our empirical function.

Optics EXPRESS

A. Appendix

Supplementary figures are included in this appendix. They comprise raw experimental details, average PSDs and equivalent θ-dependent analyses for cases not covered in the main sections.

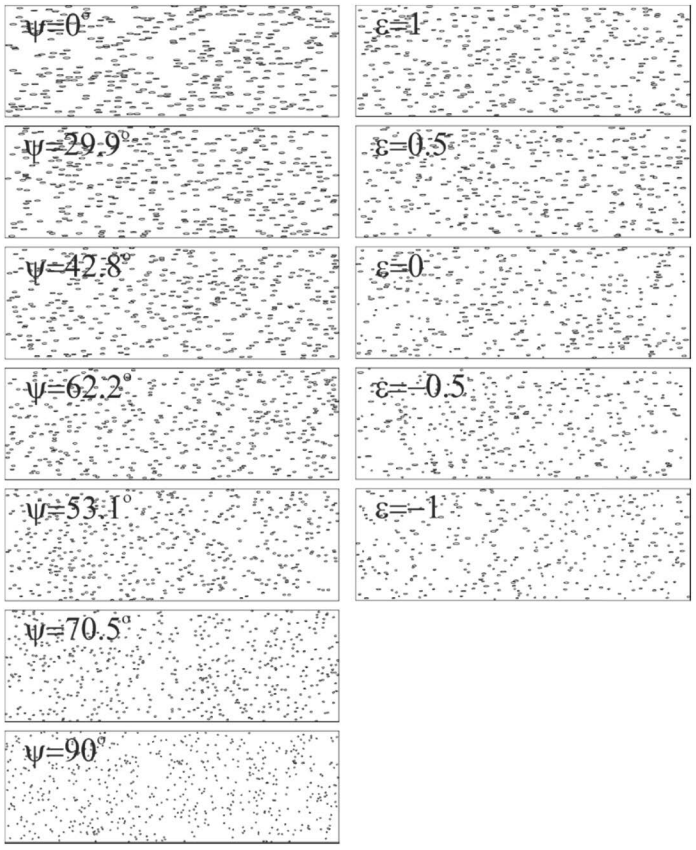

Fig. 7. Photolithographic micropillar masks for the 7 ψ angles (left) and 5 ε randomness (right).

Optics EXPRESS

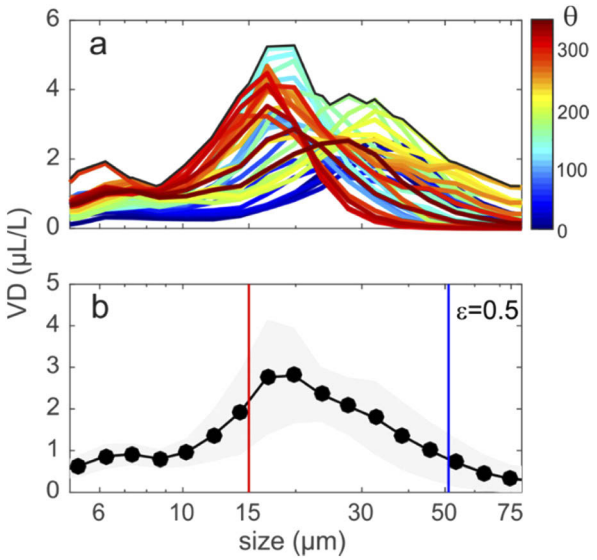

Fig. 8. a) Variation of the size spectrum with in-plane orientation θ for ε=0.5. The black line represents de envelope. b) Mean spectrum. The red and blue lines represent a and b$\perp$ dimensions. The shaded area marks the mean ± std.

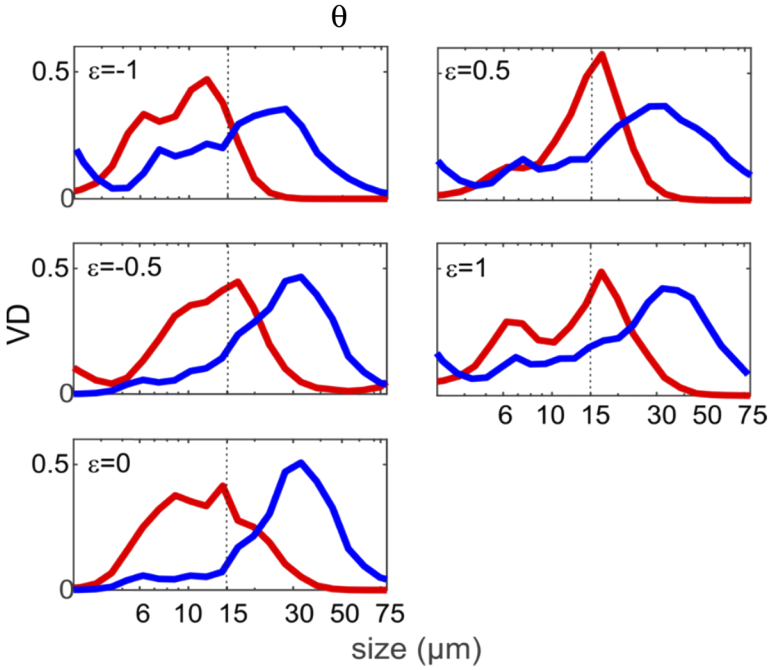

Fig. 9. PSD for random orientation distributions, in blue for orientations of 0° (or 180) in red for orientations of 90° (or 270°) in the XY plane (x-axis is in log scale).

Optics EXPRESS

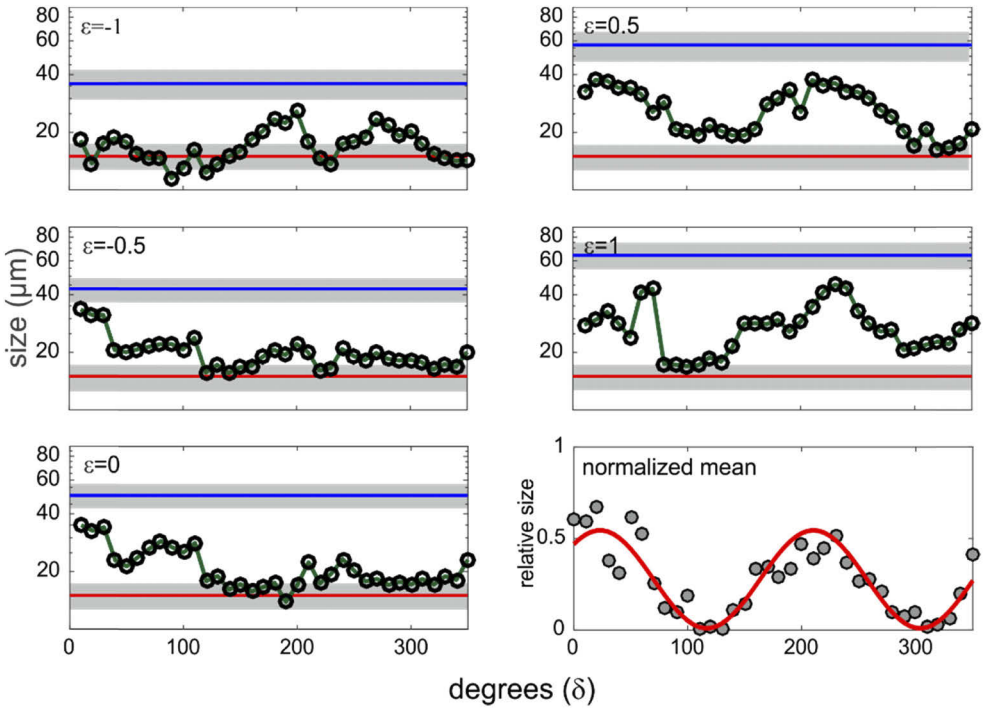

Fig. 10. Position of the main peak of the PSD (from Gaussian decomposition) for 35 orientations in the XY plane for the 5 different PDMS plates with non-uniform distributions. The red lines indicate the size of the minor axis of the micropillars, while the blue lines indicate the size of the mean value of the major axis (i.e. $< b\perp >$) in the micropillars. The normalized mean size varying from 0(=a) to 1(=b) for each θ orientation is shown in the bottom right panel. The red line corresponds to a sinusoidal fit of the data.

Optics EXPRESS

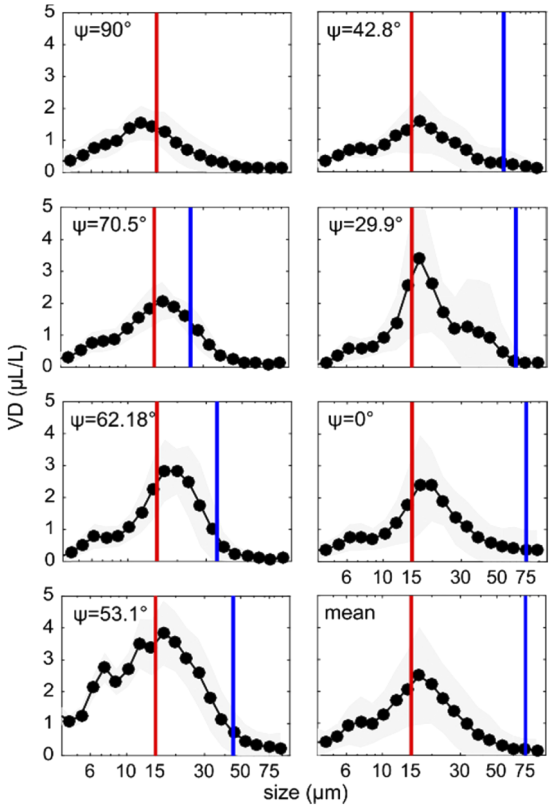

Fig. 11. Average PSD of all 35 orientations in the XY plane for each orientation in the XZ plane. The red and blue lines indicate the sizes of the minor (a) and major axis (b) of the micropillars.

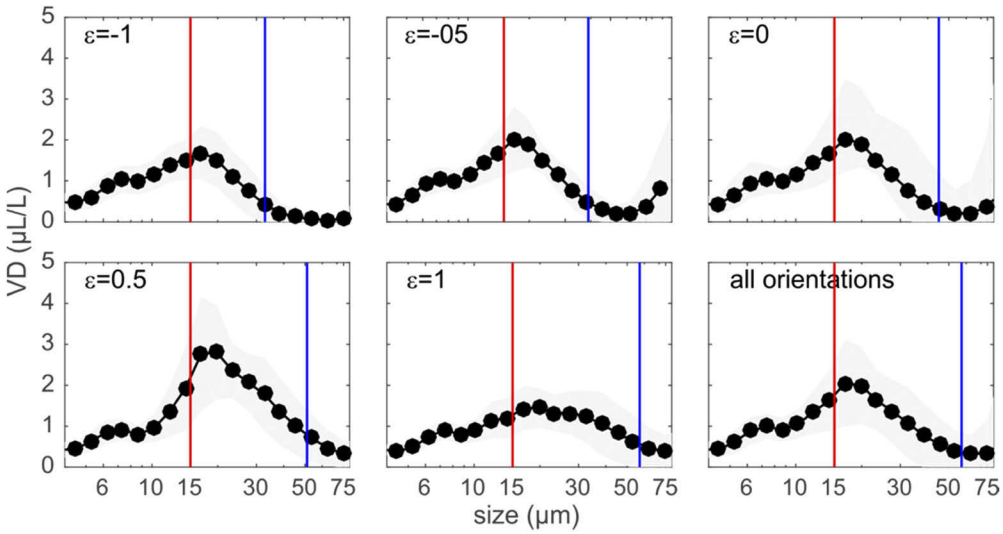

Fig. 12. Average PSD of the 35 orientations in the XY plane of the different random orientation distributions characterized by the epsilon parameter. The red lines indicate the size of the minor axis of the micropillars, while the blue line indicates the size of the average major axis of the micropillars of the random distribution.

Optics EXPRESS

Funding

SIFOMED (CTM2017-83774-P); INTERDIBIO (FIS2016-77692-C2-1-P); Ministerio de Ciencia, Innovación y Universidades; Agencia Estatal de Investigación; European Regional Development Fund; National Research Agency under the ISblue program (ANR-17-EURE-0015).

Acknowledgements

J.S. F-M received a French state aid managed by the National Research Agency under the ISblue program (ANR-17-EURE-0015). R.J. acknowledges funding by an individual postdoctoral fellowship "Juan de la Cierva – Incorporación" and by the LabEx ENS-ICFP: ANR-10-LABX-0010/ANR-10-IDEX-0001-02 PSL*.

Disclosures

The authors declare no conflicts of interest.

References

1. W. Clavano, E. Boss, L. Karp-Boss, R. N. Gibson, R. J. A. Atkinson, and J. D. M. Gordon, "Inherent Optical Properties of Non-Spherical Marine-Like Particles From Theory To Observation," Oceanogr. Mar. Biol. an Annu. Rev. **45**, 1–38 (2007).
2. E. Rienecker, J. Ryan, M. Blum, C. Dietz, L. Coletti, R. Marin, and W. P. Bissett, "Mapping phytoplankton in situ using a laser-scattering sensor," Limnol. Oceanogr.: Methods **6**(3), 153–161 (2008).
3. S. Anglès, A. Jordi, E. Garcés, M. Masó, and G. Basterretxea, "High-resolution spatio-temporal distribution of a coastal phytoplankton bloom using laser in situ scattering and transmissometry (LISST)," Harmful Algae **7**(6), 808–816 (2008).
4. G. Many, F. Bourrin, X. Durrieu de Madron, I. Pairaud, A. Gangloff, D. Doxaran, A. Ody, R. Verney, C. Menniti, D. Le Berre, and M. Jacquet, "Particle assemblage characterization in the Rhone River ROFI," J. Mar. Syst. **157**, 39–51 (2016).
5. E. J. Davies and R. Nepstad, "In situ characterisation of complex suspended particulates surrounding an active submarine tailings placement site in a Norwegian fjord," Reg. Stud. Mar. Sci. **16**, 198–207 (2017).
6. Z. P. Lee, K. P. Du, and R. Arnone, "A model for the diffuse attenuation coefficient of downwelling irradiance," J. Geophys. Res. C Ocean. **110**(C2), 1–10 (2005).
7. O. Ulloa, S. Sathyendranath, and T. Platt, "Effect of the particle-size distribution on the backscattering ratio in seawater," Appl. Opt. **33**(30), 7070 (1994).
8. F. Azam and F. Malfatti, "Microbial structuring of marine ecosystems," Nat. Rev. Microbiol. **5**(10), 782–791 (2007).
9. R. J. Gibbs, "Clay Mineral Segregation in the Marine Environment," J. Sediment. Res. **47**(1), 237–243 (1977).
10. L. M. Mayer, R. G. Keil, S. A. Macko, S. B. Joye, K. C. Ruttenberg, and R. C. Aller, "Importance of suspended participates in riverine delivery of bioavailable nitrogen to coastal zones," Global Biogeochem. Cycles **12**(4), 573–579 (1998).
11. N. M. Lawson and R. P. Mason, "Concentration of mercury, methylmercury, cadmium, lead, arsenic, and selenium in the rain and stream water of two contrasting watersheds in western Maryland," Water Res. **35**(17), 4039–4052 (2001).
12. C. F. Jago, S. E. Jones, P. Sykes, and T. Rippeth, "Temporal variation of suspended particulate matter and turbulence in a high energy, tide-stirred, coastal sea: Relative contributions of resuspension and disaggregation," Cont. Shelf Res. **26**(17-18), 2019–2028 (2006).
13. J. P. Syvitski, "Methods and Application of Particle Size Analysis Cambridge," (1991).
14. T. Allen, *Powder Sampling and Particle Size Measurement* (Chapman and Hall, 1997), 1.
15. R. A. Reynolds, D. Stramski, V. M. Wright, and S. B. Woźniak, "Measurements and characterization of particle size distributions in coastal waters," J. Geophys. Res.: Oceans **115**(C8), C08024 (2010).
16. H. Groundwater, M. S. Twardowski, H. M. Dierssen, A. Sciandra, and S. A. Freeman, "Determining size distributions and composition of particles suspended in water: A new SEM-EDS protocol with validation and comparison to other methods," J. Atmos. Ocean. Technol. **29**(3), 433–449 (2012).
17. Y. C. Agrawal and H. C. Pottsmith, "Autonomous Long-Term In-Situ Particle Sizing Using A New Laser Diffraction Instrument," Proc. Ocean. **5**, 1575–1580 (1989).
18. P. Gentien, M. Lunven, M. Lehaitre, and J. L. Duvent, "In-situ depth profiling of particle sizes," Deep Sea Res., Part I **42**(8), 1297–1312 (1995).
19. Y. C. Agrawal and H. C. Pottsmith, "Instruments for particle size and settling velocity observations in sediment transport," Mar. Geol. **168**(1-4), 89–114 (2000).
20. J. M. Sullivan and M. S. Twardowski, "Angular shape of the oceanic particulate volume scattering function in the backward direction," Appl. Opt. **48**(35), 6811–6819 (2009).
21. A. J. Bale, "In situ laser optical particle sizing," J. Sea Res. **36**, 31–36 (1996).

Optics EXPRESS

22. G. Basterretxea, A. Jordi, E. Garcés, S. Anglès, and A. Reñé, "Seiches stimulate transient biogeochemical changes in a microtidal coastal ecosystem," Mar. Ecol.: Prog. Ser. **423**, 15–28 (2011).
23. J. S. Font-Muñoz, A. Jordi, I. Tuval, J. Arrieta, S. Anglès, and G. Basterretxea, "Advection by ocean currents modifies phytoplankton size structure," J. R. Soc., Interface **14**(130), 20170046 (2017).
24. Y. C. Agrawal, A. Whitmire, O. A. Mikkelsen, and H. C. Pottsmith, "Light scattering by random shaped particles and consequences on measuring suspended sediments by laser diffraction," J. Geophys. Res.: Oceans **113**(C4), C04023 (2008).
25. T. Wriedt, "Mie theory: a review," in *The Mie Theory* (Springer, 2012), pp. 53–71.
26. C. F. Bohren and D. R. Huffman, *Absorption and Scattering of Light by Small Particles* (John Wiley & Sons, 2008).
27. L. Karp-Boss, L. Azevedo, and E. Boss, "LISST-100 measurements of phytoplankton size distribution: evaluation of the effects of cell shape," Limnol. Oceanogr.: Methods **5**(11), 396–406 (2007).
28. S. Asano and M. Sato, "Light scattering by randomly oriented spheroidal particles," Appl. Opt. **19**(6), 962–974 (1980).
29. A. Mugnai and W. J. Wiscombe, "Scattering from nonspherical Chebyshev particles. I: cross sections, single-scattering albedo, asymmetry factor, and backscattered fraction," Appl. Opt. **25**(7), 1235–1244 (1986).
30. L. Karp-Boss and E. Boss, "The elongated, the squat and the spherical: selective pressures for phytoplankton shape," in *Aquatic Microbial Ecology and Biogeochemistry: A Dual Perspective* (Springer, 2016), pp. 25–34.
31. P. Latimer, A. Brunsting, B. E. Pyle, and C. Moore, "Effects of asphericity on single particle scattering," Appl. Opt. **17**(19), 3152 (1978).
32. N. Gabas, N. Hiquily, and C. Laguérie, "Response of Laser Diffraction Particle Sizer to Anisometric Particles," Part. Part. Syst. Charact. **11**(2), 121–126 (1994).
33. G. J. Streekstra, A. G. Hoekstra, E.-J. Nijhof, and R. M. Heethaar, "Light scattering by red blood cells in ektacytometry: Fraunhofer versus anomalous diffraction," Appl. Opt. **32**(13), 2266–2272 (1993).
34. G. J. Streekstra, A. G. Hoekstra, and R. M. Heethaar, "Anomalous diffraction by arbitrarily oriented ellipsoids: applications in ektacytometry," Appl. Opt. **33**(31), 7288 (1994).
35. L. Karp-Boss and P. A. Jumars, "Motion of diatom chains in steady shear flow," Limnol. Oceanogr. **43**(8), 1767–1773 (1998).
36. S. Talapatra, J. Hong, M. McFarland, A. Nayak, C. Zhang, J. Katz, J. Sullivan, M. Twardowski, J. Rines, and P. Donaghay, "Characterization of biophysical interactions in the water column using in situ digital holography," Mar. Ecol.: Prog. Ser. **473**, 29–51 (2013).
37. A. R. Nayak, M. N. McFarland, J. M. Sullivan, and M. S. Twardowski, "Evidence for ubiquitous preferential particle orientation in representative oceanic shear flows," Limnol. Oceanogr. **63**(1), 122–143 (2018).
38. J. S. Font-Muñoz, R. Jeanneret, J. Arrieta, S. Anglès, A. Jordi, I. Tuval, and G. Basterretxea, "Collective sinking promotes selective cell pairing in planktonic pennate diatoms," Proc. Natl. Acad. Sci. U. S. A. **116**(32), 15997–16002 (2019).
39. G. Basterretxea, J. S. Font-Muñoz, and I. Tuval, "Phytoplankton orientation in a turbulent ocean: a microscale perspective," (submited).
40. S. Andrews, D. Nover, and S. G. Schladow, "Using laser diffraction data to obtain accurate particle size distributions: the role of particle composition," Limnol. Oceanogr.: Methods **8**(10), 507–526 (2010).
41. E. J. Davies, "Scattering properties of suspended particles," (2013).
42. E. Organelly, G. Dall'Olmo, R. J. W. Brewin, G. A. Tarran, E. Boss, and A. Bricaud, "The open-ocean missing backscattering is in the structural complexity of particles," Nat. Commun. **9**(1), 5439 (2018).
43. W. M. Durham and R. Stocker, "Thin phytoplankton Layers: characteristics, mechanisms and consequences," Annu. Rev. Mar. Sci. **4**(1), 177–207 (2012).